Polymer 129 (2017) 21–31

Contents lists available at ScienceDirect

Polymer

journal homepage: www.elsevier.com/locate/polymer

# Prediction of resin textural properties by vinyl/divinyl copolymerization modeling

Leandro G. Aguiar [a, *], Juliana O.V. Moura [a], Thiago R. Theodoro [a], Turibio G.S. Neto [b], Vinícius M.P. Lopes [b], Joslaine R. Dias [a]

[a] Department of Chemical Engineering, Engineering School of Lorena, University of São Paulo, 12602-810, Lorena, SP, Brazil
[b] Combustion and Propulsion Associated Laboratory, National Institute for Space Research, 12630-000, Cachoeira Paulista, SP, Brazil

ARTICLE INFO

*Article history:*
Received 6 August 2017
Received in revised form
16 September 2017
Accepted 18 September 2017
Available online 19 September 2017

*Keywords:*
Modeling
Polymerization
Gel
Specific surface area
Resin

ABSTRACT

The production of polymeric resins through free-radical copolymerization is an interesting procedure from an economic standpoint; however, its mathematical representation is of great complexity. In the present study, modeling tools were used to describe the copolymerization of styrene with ethylene glycol dimethacrylate (EGDMA) beyond the gel point. Balance of species and sequences, method of moments, and numerical fractionation technique were applied in the model's kinetic description. Diffusion effects were also taken into account. The concept of elementary gel structures (EGSs) was used in order to predict textural properties of polymer particles, such as specific surface area and swollen gel volume. Suspension copolymerizations were carried out in the presence of toluene/heptane mixtures, and data on these reactions were used to assess the model's predictability. Reactivity parameters showed similarities to styrene/divinylbenzene systems. Agreement between the model and experimental data improved when diffusion effects were considered. The fitted apparent coiling factors for dry particles were found in the range of 0.368–0.406, and a linear correlation was obtained between this parameter and toluene fraction (a good solvent), being consistent with the pore formation phenomenon.



## 1. Introduction

Ion exchange resins represent a central element in many academic and industrial applications, such as deionization [1], removal of oil and heavy metals from water [2], and heterogeneous catalysis. The latter has been a subject of recent studies comprising sulfonated styrene-based copolymers [3], esterifications [4], etherifications [5], and biodiesel production [6]. When polymer gels are synthesized for these applications, not only information on reaction kinetics [7–10] and diffusion phenomena [11,12] but also information on morphological and structural aspects are relevant to obtaining the desired performance. In porous polymer particles, larger surface areas allow a higher number of catalytic sites; therefore, the control of this property in function of polymerization variables is of great interest. In this context, [13] synthesized microporous polymer networks and developed a procedure to control the pore size and surface area of the material by varying synthesis conditions [13]. Recent experimental studies have been carried out on functionalized polymer supports with high surface areas [14], interpenetrating polymer networks with adsorption properties [15], and the effect of cross-linking density on polymer morphology [16]. Despite the predictability provided by the methods presented in these references, these types of experimental studies use an empirical approach with no detailed theory about the synthesis phenomena. An earlier modeling study based on the concept of elementary gel structures (EGSs) was developed for the prediction of specific surface area during gel synthesis [17]. The referred model provides a theoretical foundation on the formation of surface area based on the estimated radius of gyration of gel molecules. Despite the conceptual background developed in this reference, the predictability of specific surface area depends on the correlation between the EGS coiling factor and polymerization variables, which is an unsolved issue. The porosity of gel particles has also been a subject of modeling studies based on the method of moments and numerical fractionation technique [18,19]. Literature approaches for pore volume prediction involve the calculation of phase separation by using modified Flory equations, which runs into convergence problems, demanding considerable

* Corresponding author.
*E-mail address:* leandroaguiar@usp.br (L.G. Aguiar).

https://doi.org/10.1016/j.polymer.2017.09.042
0032-3861/

computational effort. For applications in which polymer swelling occurs (e.g., size exclusion chromatography [20], catalysis [21]), not only the fixed pore volumes but also the swelling index plays an important role. Thus, a mathematical model for predicting the swollen gel volume can represent an interesting tool for the design of polymer resins with specific properties. In spite of some advances in the modeling of particle macrostructure, a complete mathematical representation of the phenomena involving gel formation and its properties remains a challenge. In the current state-of-art of polymerization modeling, the connection between basic (rates of reaction) and applied (material properties) science is not well established. Hence, there is a need for a mathematical model that simultaneously simulates reaction variables (e.g., conversion, species concentration) and textural properties. The aim of this work was to develop a mathematical model for vinyl/divinyl copolymerization based on the balance of species and sequences, method of moments, numerical fractionation technique, diffusion-controlled rate coefficients, and elementary gel structures. Furthermore, the model's ability to predict specific surface area, swollen gel volume, monomer conversion, and the weight fraction of gel was assessed.

## 2. Experimental

### 2.1. Copolymerization procedure

Suspension copolymerizations of styrene/EGDMA (15% organic phase/85% aqueous phase, vol%) were carried out in a 1 L jacketed glass reactor at 80 °C under mechanical agitation at 350 rpm. The reactions were conducted in the presence of toluene/heptane mixture, initiated by 1 mol% of benzoyl peroxide (BPO) in the organic phase, which was stabilized by 1 wt% of polyvinyl alcohol (PVA) in the aqueous phase. The dosages of each experiment are summarized in Table 1.

Samples of 40 mL were withdrawn at prescribed times and received the addition of 10 mL of a 1.4 wt% hydroquinone solution in methanol in order to cease free radical reactions. Analyses of conversion, weight fraction of gel, specific surface area, fixed pore volume, and swelling index were carried out by using the procedures described in the following topics. All symbols used in the equations and their meaning are listed in the Symbology section.

### 2.2. Monomer conversion

Each sample collected from the reactor was submitted to a drying process at 60 °C until constant weight. Total monomer conversion was calculated by using gravimetric analysis, as shown in Equation (1).

**Table 1**
Feeding concentrations.

| Run | $Y_M$ | $Y_{EGDMA}$ | $Y_{TOL}$ |
|---|---|---|---|
| A | 0.3 | 0.1 | 0.4 |
| B | 0.3 | 0.3 | 0.5 |
| C | 0.3 | 0.5 | 0.6 |
| D | 0.4 | 0.1 | 0.5 |
| E | 0.4 | 0.3 | 0.6 |
| F | 0.4 | 0.5 | 0.4 |
| G | 0.5 | 0.1 | 0.6 |
| H | 0.5 | 0.3 | 0.4 |
| I | 0.5 | 0.5 | 0.5 |

$Y_M$: Volumetric fraction of monomers in the organic phase; $Y_{EGDMA}$: Molar fraction of EGDMA in the monomer mixture; $Y_{TOL}$: Volumetric fraction of toluene in the toluene/heptane mixture.

$$X = \frac{w_d - w_s y_{PVA} - w_{HQ}}{y_{Mon} w_s} \quad (1)$$

### 2.3. Weight fraction of gel

After the drying process, the polymer was submitted to a series of extractions with tetrahydrofuran (THF), followed by filtration (pore size = 7.5 μm) and drying in order to remove soluble chains. When constant weight was achieved, the weight of the gel was registered, and the experimental gel fraction was calculated.

### 2.4. Specific surface area

The specific surface area of gel particles was determined by $N_2$ adsorption at −196 °C and 1 atm, according to the classic method developed by Brunauer et al. [22]. Preceding the adsorption measurements, particles were heated for 2 h at 80 °C under $1.33 \times 10^{-6}$ kPa vacuum. The equipment used was a Nova 1000 Quantachrome.

### 2.5. Fixed pore volume

The fixed pore volume ($V_P$) of polymer particles was determined through the water-uptake method [23,24]. About 0.5 g of dry polymer was washed with distilled water and placed on a filter paper inside a plastic tube. Then, two centrifugation/washing (water/methanol) cycles were conducted, and the fixed pore volume was calculated by determining the amount of retained water.

### 2.6. Swelling index

Approximately 0.5 g of dry gel was swollen in excess THF (about 10 mL) for 24 h. The wet gel was placed in a Petri dish and its weight was measured over time. The initial linearity of the mass loss curve indicated the evaporation of excess THF. When the mass profile became curvilinear, the gel was considered to be shrinking. Swelling equilibrium was considered when the mass profile lost 1% of its linearity ($R^2 < 0.99$ for linear regression). Then, the swelling index was determined by dividing the weight of the swollen gel in equilibrium by the dry weight.

$$Sw = \frac{w_{sw}}{w_d} \quad (2)$$

### 2.7. Swollen gel volume

The swollen gel volume defined herein refers to the volume of gel swollen in THF per gram of polymer gel. Its experimental value was calculated in function of the previously defined variables, as follows.

$$V_{sw} = Sw\left(V_P + \frac{1}{\rho_P}\right) \quad (3)$$

## 3. Modeling

A previously developed mathematical model based on the balance of species and sequences, method of moments, and numerical fractionation technique [17] was complemented with the prediction of swollen gel volume and applied to styrene/EGDMA

copolymerization. The reaction steps considered in the model are listed in Table 2.

Details on the balance of species, moments, and sequences are presented in the Appendix.

### 3.1. Prediction of specific surface area

The specific surface area of the copolymer particles was mathematically modeled by using the elementary gel structure theory [17], as described in Equations (4)–(13).

$$\frac{dG}{dt} = k_{PP} Y_0^n Q_1^n + k_t Y_0^n Y_0^n - k_{CG} G^2 \tag{4}$$

$$R_{g1} = \beta_1 M_G^{A_1} \tag{5}$$

$$A_1 = 0.1846 Y_{Tol} + 0.409 \tag{6}$$

$$\beta_1 = \gamma_1 \rho_{CL}{}^{\gamma_2} \tag{7}$$

$$\rho_{CL} = \frac{U_2 - PDB}{Q_1} \tag{8}$$

$$k_{CG} = k_{CG0}[R]_G [PDB]_G \rho_{CL}{}^{\gamma_2} M_G^{A_1} \tag{9}$$

$$M_G = \frac{W_g Q_1 \overline{M_M}}{G} \tag{10}$$

$$\overline{M_M} = \frac{U_1 M_{M1} + U_2 M_{M2}}{U_1 + U_2} \tag{11}$$

$$R_{g2} = \beta_2 M_G^{A_2} \tag{12}$$

$$SA = \frac{G N_A \left(4\pi R_{g2}^2\right)}{10^{18} W_g Q_1 \overline{M_M}} \tag{13}$$

This methodology was first proposed for a styrene/divinylbenzene copolymerization system [17] and, in this work, was extended to styrene/EGDMA since it is also a vinyl/divinyl copolymerization.

### 3.2. Prediction of swollen gel volume

The theoretical swollen gel volume in the reaction medium can also be estimated by using the concept of elementary gel structures. The predicted swollen volume ($V_{sw}^p$) is a function of model variables, as shown in Equation (14),

$$V_{sw}^p = \frac{1000}{G M_G} \varphi \tag{14}$$

where $\varphi$ is a conversion factor to transform $cm^3$ of gel swollen in the reaction medium to $cm^3$ of gel swollen in THF. Based on the concept of radius of gyration (Eq. (5)), this volume ratio can be expressed as shown in Equation (15), in which subscript 3 refers to THF.

$$\varphi = \left(\frac{\beta_3}{\beta_1} M_G^{A_3 - A_1}\right)^3 \tag{15}$$

During the aqueous suspension copolymerization, the process of breaking/coalescence of particles is responsible for the redistribution of solvent as the gel is being formed and absorbs organic phase. In this interparticle mass transfer process, it is natural that excess solvent from particles containing tottally swollen gel be transferred to particles containing gel molecules that are still absorbing fluids (molecules that have not yet reached equilibrium). Considering this mechanism, the EGSs are expected to reach swelling equilibrium as the reaction proceeds, allowing, as an approximation, the comparison between $V_{sw}$ and $V_{sw}^p$.

**Table 2**
Styrene/EGDMA copolymerization steps considered in the model.

| Reaction | Chemical equation |
|---|---|
| Initiator decomposition | $I \xrightarrow{k_d} 2R_0$ |
| Monomer propagation | $R_{r,i} + M_j \xrightarrow{k_{pij}} R_{r+1,j}; j = 1,2$ |
| Cross-linking | $R_{r,i} + P_s \xrightarrow{k_{pi3}} R_{r+s,3}$ |
| Initiation | $R_0 + M_j \xrightarrow{k_{ij}} R_{1,j}; j = 1,2$ |
| PDB initiation | $R_0 + P_s \xrightarrow{k_{i3}} R_{s,3}$ |
| Termination by combination | $R_{r,i} + R_{s,j} \xrightarrow{k_t} P_{r+s}$ |

PDB: Pendant double bond. Subscripts 'r' and 's' represent the number of monomer units. The numbers are related to the following: 1 - Styrene, 2 - EGDMA, 3 - PDB.

## 4. Results and discussion

The physical properties of copolymer particles collected at prescribed reaction times (180, 240, 300, and 360 min) were measured and are summarized in Table 3.

It can be observed that, in general, fixed pore volumes increase as specific surface areas increase, as expected. The swelling indices of the produced gel particles were lower when smaller monomer fractions were fed to the copolymerization (Runs A, B, and C) than when higher monomer fractions were used (Runs G, H, and I). Overall, the data presented in Table 3 show acceptable coherence and can be used to assess the validity of the mathematical model.

Figs. 1–3 show the experimental and modeling results of specific surface area and swollen gel volume.

The background knowledge on specific surface area modeling is based on elementary gel structures, which consist of insoluble polymer molecules that are formed during the copolymerization reaction [17]. When two EGSs react by cross-linking or termination, the total exposed surface area is reduced, explaining the profiles observed in Figs. 1–3. The model predictions of swollen gel volume presented decreasing trend over time. This behavior is feasible because this volume is relative to the weight of the gel, which increases as the reaction time increases. Therefore, the swollen gel volume diverges at the gelation point, in which the gel weight tends to zero. It is important to point out that, in the specific surface area and swollen gel volume model profiles, the peaks observed near the gel points (before 180 min) are related to the formation of the first gel structures at a molecular level, i.e., macroscopic gel particles cannot be observed at this interval. In spite of mass variation detected by gravimetric analyses, gel particles obtained after extractions with THF could not be visualized nor removed from the filter paper. This limitation occurred for most of the samples collected before 180 min, probably due to the entrapment of very small particles in the filter pores. Nonetheless, the determination of gel point is quite subjective. Different techniques, such as simple extraction with toluene [25], Soxhlet extraction [26], and size exclusion chromatography (SEC) [27] can be used; however, different gelation points can be obtained according to the pore size of the filter used in the analysis. In order to keep the coherence with previous experimental/modeling studies [28,29], the gel fraction results presented herein were determined by simple extractions

**Table 3**
Physical characteristics obtained from particle analyses.

| | Specific surface area ($m^2/g$) | | | | Fixed pore volume ($cm^3/g$) | | | | Swelling Index | | | |
|---|---|---|---|---|---|---|---|---|---|---|---|---|
| Time (min) | 180 | 240 | 300 | 360 | 180 | 240 | 300 | 360 | 180 | 240 | 300 | 360 |
| Run A | 0.0 | 0.0 | 0.0 | 0.0 | 0.13 | 0.25 | 0.00 | 0.15 | 2.88 | 1.39 | 4.35 | 2.69 |
| Run B | 62.9 | 53.2 | 70.8 | 50.4 | 0.81 | 0.72 | 0.00 | 0.00 | 3.22 | 3.42 | 3.22 | 3.63 |
| Run C | 65.6 | 115.6 | 140.3 | 137.9 | 0.76 | 0.71 | 0.67 | 1.11 | 4.72 | 3.82 | 4.55 | 2.48 |
| Run D | 0.0 | 0.0 | 0.0 | 0.0 | 0.06 | 0.05 | 0.01 | 0.15 | 1.99 | 1.63 | 1.57 | 2.02 |
| Run E | 71.1 | 64.6 | 61.5 | 58.8 | 0.47 | 0.00 | 0.25 | 0.46 | 3.13 | 1.99 | 1.99 | 2.69 |
| Run F | 22.4 | 31.2 | 22.6 | 30.4 | 1.86 | 1.31 | 0.98 | 1.07 | 3.03 | 2.05 | 2.57 | 1.77 |
| Run G | 0.0 | 0.0 | 0.0 | 0.0 | 0.57 | 0.20 | 0.62 | 0.01 | 1.30 | 1.84 | 1.37 | 3.24 |
| Run H | 2.1 | 0.1 | 5.4 | 2.8 | 0.86 | 0.59 | 0.85 | 0.16 | 1.13 | 1.88 | 1.91 | 2.13 |
| Run I | 81.3 | 75.9 | 78.4 | 71.9 | 0.28 | 0.36 | 0.39 | 0.53 | 1.22 | 1.65 | 1.27 | 1.77 |

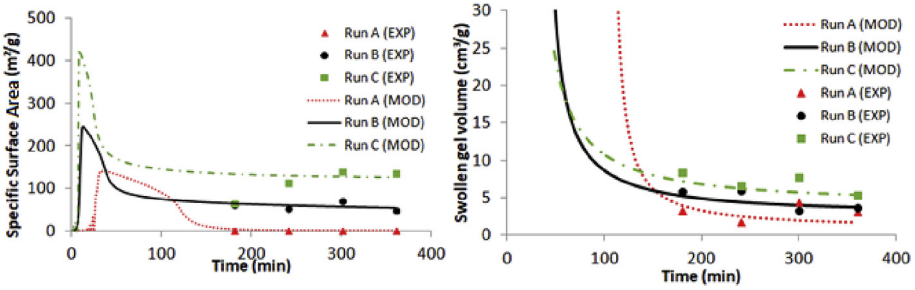


**Fig. 1.** Experimental and modeling results of specific surface area and swollen gel volume (Runs A to C).

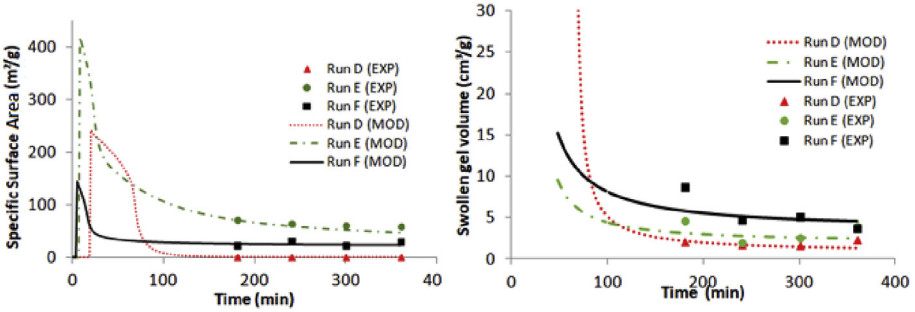


**Fig. 2.** Experimental and modeling results of specific surface area and swollen gel volume (Runs D to F).

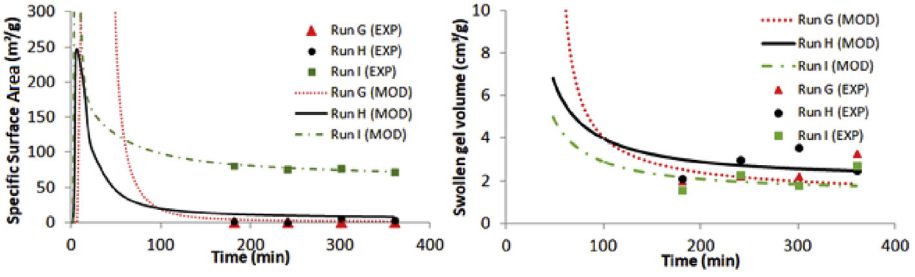


**Fig. 3.** Experimental and modeling results of specific surface area and swollen gel volume (Runs G to I).

with THF, as described in the experimental section. Due to the uncertainties and limitations related to the gel point, the present study focused on the final textural properties obtained after stabilization, i.e., the period from 180 to 360 min, observed in Figs. 1–3. Furthermore, for applications of interest, such as heterogeneous catalysis, the polymer support must be a macrogel with appreciable chemical and mechanical resistance. Based on the present process conditions and experimental observations, these characteristics probably cannot be obtained before 180 min of reaction. Therefore, the model validation in terms of textural properties was carried out only for the stable regions observed in Figs. 1–3, in which the gel particles were completely formed, visible, and useful for application purposes. Fig. 4 depicts the model fittings considering the averages of textural properties in the range of 180–360 min.

Previous studies indicate that styrene/dimethacrylate copolymerization systems are likely to present effects related to viscosity phenomena (e.g, diffusion effects). Shah et al. studied this

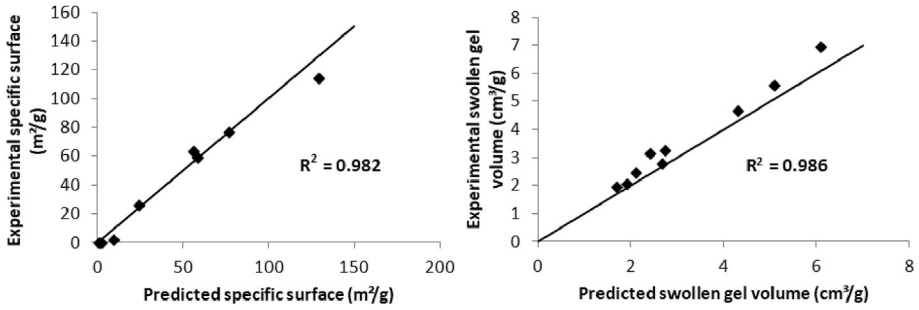


**Fig. 4.** Comparison between experimental and predicted values of specific surface area and swollen gel volume. Average values for the range of 180–360 min.

copolymerization with dimethacrylate dosages up to 20% using styrene autoinitiation (without an initiator). The results were a small radical generation rate, longer chains, and, consequently, a considerable autoacceleration effect [10,32,33]. Depending on the characteristics of the compounds involved in the polymerization, the efficiency of BPO may assume very low values. Imoto et al. (1955) found an efficiency of 0.25 for BPO in the presence of dimethylaniline [34]. Given the viscous nature of the styrene/dimethacrylate systems mentioned herein, a cage effect is expected to occur during the process. Hence, the values f = 0.25 and Cp = 0.05 (low cross-linking reactivity) found through curve fitting are probably associated with the relatively high amount of EGDMA fed to the reactions (up to 50%), resulting in high viscosities. Furthermore, BPO was not pretreated before its use; thus, moisture and impurities may have affected its fed concentrations. Despite the parameters related to diffusion-limited steps, the other reactivity ratios of this vinyl/divinyl copolymerization system were considered to be the same as for a styrene/DVB system, as shown in Table 4. The values for the model parameters $A_2$ and $A_3$ were obtained through curve fitting and are reported in Table 5.

The parameter $A_2$ is related to the conformation of EGSs in the dry state. It is the exponent of the radius of gyration expression (Eq. (12)), valid for soluble polymer molecules and extrapolated for polymer gels in the present study. The coiling degree of polymer molecules depends on their affinity to the solvent with which they are in contact [31]. In the present copolymerization runs, solvent mixtures with more toluene (a good solvent) are expected to provide bigger EGSs when compared to mixtures with more heptane (a poor solvent). Thus, the fitted value of $A_2$ was correlated with the variable $Y_{TOL}$ in order to verify its trend, as shown in Fig. 5.

**Table 5**
Fitted values of $A_2$ and $A_3$.

| Run | A | B | C | D | E | F | G | H | I |
|---|---|---|---|---|---|---|---|---|---|
| $A_2$ | 0.368 | 0.387 | 0.406 | 0.386 | 0.406 | 0.370 | 0.425 | 0.390 | 0.406 |
| $A_3$ | 0.497 | 0.532 | 0.556 | 0.520 | 0.530 | 0.522 | 0.539 | 0.511 | 0.529 |

A linear correlation can be observed in Fig. 5, which indicates that $A_2$ is directly proportional to the fraction of toluene in the solvent mixture, as expected. The equations presented in Fig. 5 were found by linear regression and are very similar to Equation (6), which was used to calculate parameter $A_1$ for the estimative of the radius of gyration of EGSs during the reaction. Conclusively, the correlation of the coiling parameter in the dry state ($A_2$) with solvent composition seems to be a consequence of interactions between EGSs and the solvent mixture during the reaction, in which the coiling parameter in the swollen state ($A_1$) is also directly proportional to $Y_{TOL}$.

The fitted values of $A_3$ were close to 0.565, which is the coiling factor of soluble linear polystyrene chains in THF ($A_{THF}$) [35], as illustrated in Fig. 6.

Since this study focused on non-linear polymer molecules, a lower radius of gyration is expected in comparison to linear chains,

**Table 4**
Model parameters.

| Reaction | Rate constant | Ref. |
|---|---|---|
| BPO decomposition | $k_d = 6.94x10^{13} exp\left(-\frac{122300}{RT}\right)\ s^{-1}$ | [28,30] [a] |
| | f = 0.25 | |
| Styrene propagation | $k_{p11} = 4.27x10^{7} exp\left(-\frac{32500}{RT}\right)\ \frac{L}{mol\ s}$ | [28,30] |
| Initiation | $k_{1j} = k_{p1j}\ (1 \le j \le 3)$ | [28,30] |
| Radical termination | $\frac{k_{p11}}{k_t^{0.5}} = 426.4 exp\left(-\frac{26000}{RT}\right)\ \frac{L}{mol\ s}$ | [28,30] |
| Cyclization of styrene radical for 3 monomeric units | $k_{p1,3}^{c} = 2.13x10^{7} exp\left(-\frac{32500}{RT}\right)\ s^{-1}$ | [28] |
| EGS combination | $k_{CG0} = 1.4x10^{-3}$ | [17] |
| Reactivity ratios | $C_P = 0.05$ | [a] |
| | $r_{12} = \frac{k_{p11}}{k_{p12}} = 0.43$ | [28,30] |
| | $r_{13} = \frac{k_{p11}}{k_{p13}} = \frac{2r_{12}}{C_P}$ | [28,30] |
| | $r_{2i} = \frac{k_{p2i}}{k_{p1i}} = 0.77\ (1 \le i \le 3)$ | [28,30] |
| | $r_{3i} = \frac{k_{p3i}}{k_{p1i}} = 0.59\ (1 \le i \le 3)$ | [28,30] |
| $R_{g2}$ equation coefficient | $\beta_2 = 0.03$ | [31,17] |
| $\beta_1$ equation coefficient | $\gamma_2 = -12$ | [31,17] |
| $\beta$ ratio | $\frac{\beta_3}{\beta_1} = 0.6$ | [a] |

[a] Fitted in the present study.

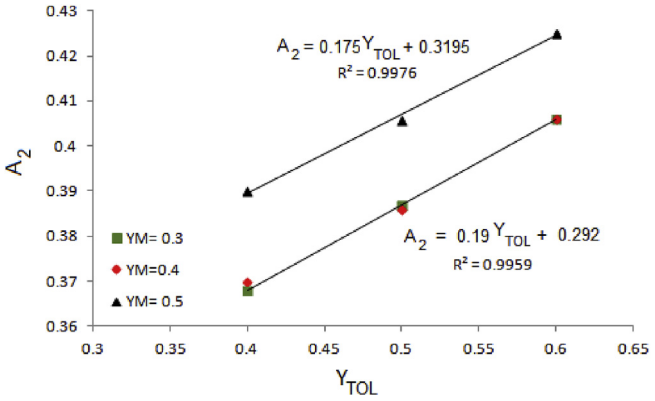


**Fig. 5.** Correlations between $A_2$ and toluene fraction ($Y_{TOL}$).

which explains the slight discrepancy observed in Fig. 6. According to literature data, $\beta_{THF} = 0.0181$ for linear polystyrene in THF [35]. Assuming, as an estimative, that this value can also be applied for styrene-co-EGDMA gels, then $\beta_3 = 0.0181$. The ratio $\frac{\beta_3}{\beta_1} = 0.6$ was fitted for all the cases studied herein, which results in $\beta_1 \cong 0.03$, indicating no considerable difference in the value of parameter $\beta$ when comparing styrene-EGDMA gels in the dry state to gels in a toluene/heptane solution ($\beta_1 \cong \beta_2$).

The present model provides a typical conversion profile when termination and cross-linking rate coefficients ($k_t$ and $k_{pi3}$, respectively, from Table 4) are considered constant along the reaction conversion. This simplified approach provided the conversion and gel fraction results shown in Fig. 7.

A slight autoacceleration effect can be observed at about 150 min of reaction in some experiments, as depicted in Fig. 7a. Runs D and G were conducted with the lowest level of EGDMA ($Y_{EGDMA} = 0.1$) of the present set of experiments. Gel fractions are expected to reach lower values as the amount of cross-linker fed to the reactor is reduced. This behavior is observed in Fig. 7b, in which the profile of Run D ($Y_{EGDMA} = 0.1$) reaches lower maximum values in comparison with the profiles of Runs B and C ($Y_{EGDMA} = 0.5$). On the other hand, an increase in monomer concentration favors gel formation, as observed in Run G profiles. These trends were observed in the experimental profiles and were reasonably corroborated by the model curves. Nevertheless, refinements in the model were needed in order to obtain a better fitting for the variables conversion and weight fraction of gel. As previously mentioned, styrene/EGDMA copolymerization systems are usually affected by diffusion effects. Thus, the required refinements in the present model were made by including a diffusion-limiting approach, considering that reactions involving the combination of

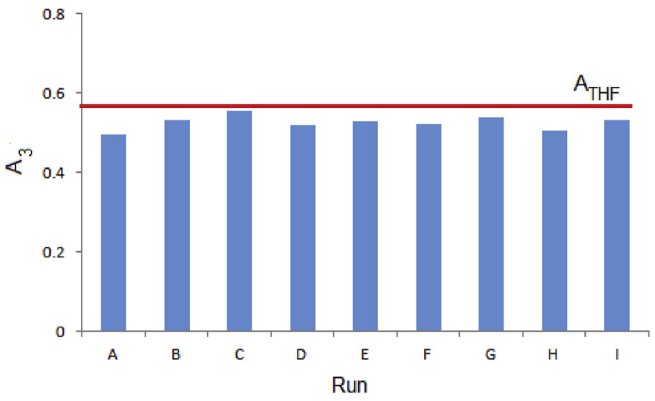


**Fig. 6.** Comparison between $A_{THF}$ and $A_3$ fitted values.

two polymer molecules (cross-linking and termination) have variable rate coefficients throughout the process. The termination rate coefficient ($k_t^*$) was written as an exponential function of the conversion, as described for a similar system [10], and this approach was also applied for the cross-linking rate coefficient ($k_{p13}^*$). The parameters $k_{p23}^*$ and $k_{p33}^*$ were calculated through the reactivity ratios listed in Table 4. Equations (16) and (17) show the referred correlations.

$$k_t^* = k_t exp(\alpha_t X) \left(\frac{L}{mol\ min}\right) \tag{16}$$

$$k_{p13}^* = 70 exp(\alpha_c X) \left(\frac{L}{mol\ min}\right) \tag{17}$$

Fig. 8 illustrates the simulations considering Equations (16) and (17) in the model.

In Fig. 8a, a Trommsdorff-Norrish effect can be observed at about 150 min for Runs C, D, and G, which can be represented by adjusting the parameter $\alpha_t$. In Run B, no pronounced autoacceleration effect was observed, and its conversion profile could be simulated with a constant $k_t$ ($\alpha_t = 0$). The experimental gel formation behavior suggests that a high cross-linking rate is obtained at the beginning $\left(k_{p13}^* = 70\ \frac{L}{mol\ min}\right)$, and the rate coefficient decreases as monomer conversion increases, providing values of $\alpha_c$ in the range of −2 to −3.8. The parameters $\alpha_t$ and $\alpha_c$ indicate how sharp the exponential decrease in the referred coefficients is along the conversion. Despite the difference in the systems, the values fitted for $\alpha$ parameters are close to those achieved for thermally-initiated styrene/EGDMA copolymerizations [10].

The diffusion effects included in these additional simulations did not significantly affect the specific surface area and swollen gel volume predictions. The major discrepancies observed when comparing Figs. 7 and 8 are in the conversion predictions. However, the textural properties are mainly related to the fraction of gel formed along the process. Small differences are obtained when comparing Figs. 7b and 8b, which led to specific surface area and swollen gel volume predictions very similar to those plotted in Figs. 1–3.

## 5. Conclusion

A mathematical model for predicting specific surface area and swollen gel volume of styrene-co-EGDMA particles during copolymerization was conceived, and its predictions were compared with experimental data. Acceptable agreement between predicted and experimental specific surface areas was obtained with fitted values of $A_2$ in the range of 0.368–0.406, which is below the value of 0.5 for unperturbed linear chains, as expected. In terms of textural properties, the model could be validated with experimental data obtained for visible particles (region with stable characteristics). Furthermore, similar linear correlations between coiling factor and toluene fraction ($Y_{TOL}$) were verified for swollen particles in the reaction medium ($A_1$) and also for the resulting product after drying ($A_2$). Moreover, the swollen gel volume predictions provided reasonable agreement by adjusting the coiling factor $A_3$. The value fitted for this parameter was slightly below the coiling factor of linear polystyrene in THF, as expected. The other parameters (e.g., reactivity ratios, rate coefficients) presented similar values in comparison to the styrene/DVB copolymerization system. In addition to textural properties, the present model provided fair predictions of gel fraction and monomer conversion, which could be improved by considering diffusion-controlled rate constants. Additionally, the present model can also be used to

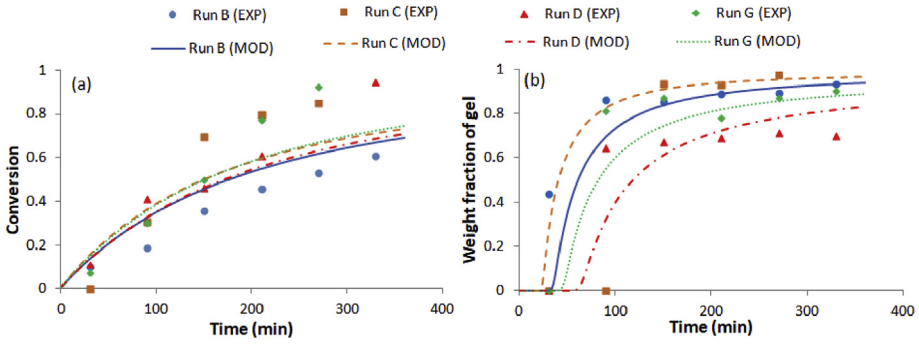


**Fig. 7.** Conversion and gel fraction results obtained with data from Table 4.

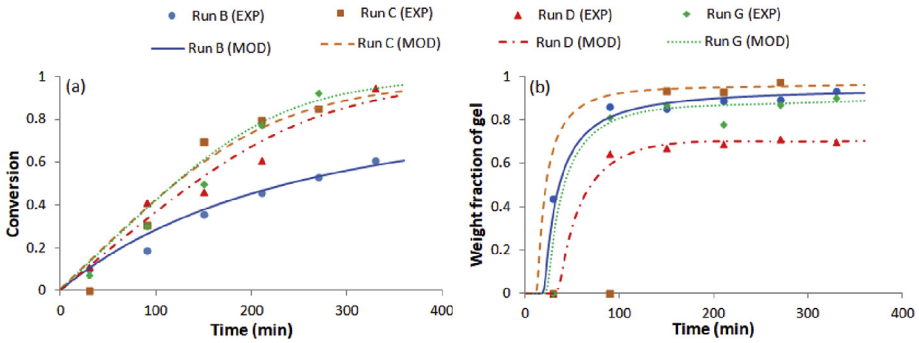


**Fig. 8.** Simulations considering autoacceleration effects. f = 0.15; $\alpha_t$ = 0 (Run B), −3.3 (Run C), −3.3 (Run D), −3.5 (Run G); $\alpha_c$ = −2 (Run B), −3.4 (Run C), −3.8 (Run D), −3.2 (Run G).

estimate average molecular weights, concentration of species, polymer groups, and cyclic chains. In conclusion, the developed mathematical model constitutes an interesting tool for the design of customized resins and provides subsidies for further studies on the estimation of other properties, such as average pore diameter, that are useful for specific applications, such as support for catalysts.

## Acknowledgments

The authors would like to thank FAPESP for the financial support (Grant No. 2014/22080-9).

## APPENDIX

### *A1. Pseudo-kinetic rate constants*

$$k_P = \sum_{i=1}^{3} f_{Ri} \sum_{j=1}^{2} k_{pij} f_{Mj} \tag{A1}$$

$$k_I = \sum_{j=1}^{2} k_{Ij} f_{Mj} \tag{A2}$$

$$k_{PP} = \sum_{i=1}^{3} f_{Ri} k_{pi3} \frac{PDB}{Q_1} \tag{A3}$$

$$k_{IP} = k_{I3} \frac{PDB}{Q_1} \tag{A4}$$

$f_{Ri}$: Fraction of radicals of type 'i'.
*PDB*: Concentration of pendant double bonds.

$$f_{Mj} = \frac{M_j}{M} \; (1 \leq \mathrm{j} \leq 2) \tag{A5}$$

$$M = M_1 + M_2 \tag{A6}$$

### *A2. Balance of species*

$$R_0 = \frac{2fk_dI}{k_I M + k_{IP} Q_1} \tag{A7}$$

$$\frac{dI}{dt} = -k_d I \tag{A8}$$

$$\frac{dM_1}{dt} = -\left[k_{I1} R_0 + Y_0 \sum_{i=1}^{3} k_{pi1} f_{R1}\right] M_1 \tag{A9}$$

$$\frac{dM_2}{dt} = -\left[k_{I2} R_0 + Y_0 \sum_{i=1}^{3} k_{pi2} f_{R2}\right] M_2 \tag{A10}$$

$$\frac{dPDB}{dt} = \left[k_{I2} R_0 + Y_0 \sum_{i=1}^{3} k_{pi2} f_{Ri}\right] M_2 - \left[k_{I3} R_0 + Y_0 \sum_{i=1}^{3} k_{pi3} f_{Ri}\right] PDB - RC \tag{A11}$$

*A3. Balance of moments*

$$Y_k = \sum_{r=1}^{\infty}\sum_{i=1}^{3} r^k R_{r,i} \tag{A12}$$

$$Q_k = \sum_{r=1}^{\infty} r^k P_r \tag{A13}$$

$$Y_0 = \sqrt{\frac{k_I R_0 M + k_{IP} R_0 Q_1}{k_t}} \tag{A14}$$

$$\frac{dQ_0}{dt} = -k_{IP} R_0 Q_1 - k_{PP} Y_0 Q_1 + \frac{1}{2} k_t Y_0^2 \tag{A15}$$

$$\frac{dQ_1}{dt} = k_I R_0 M + k_P Y_0 M \tag{A16}$$

Generation Zero

$$Y_0^0 = \frac{k_I R_0 M}{k_{PP} Q_1 + k_t Y_0} \tag{A17}$$

$$Y_1^0 = \frac{k_I R_0 M + k_P M Y_0^0}{k_{PP} Q_1 + k_t Y_0} \tag{A18}$$

$$Y_2^0 = \frac{k_I R_0 M + k_P M\left(2Y_1^0 + Y_0^0\right)}{k_{PP} Q_1 + k_t Y_0} \tag{A19}$$

$$\frac{dQ_0^0}{dt} = -k_{IP} R_0 Q_1^0 - k_{PP} Y_0 Q_1^0 + \frac{1}{2} k_t Y_0^0 Y_0^0 \tag{A20}$$

$$\frac{dQ_1^0}{dt} = -k_{IP} R_0 Q_2^0 - k_{PP} Y_0 Q_2^0 + k_t Y_0^0 Y_1^0 \tag{A21}$$

$$\frac{dQ_2^0}{dt} = -k_{IP} R_0 Q_3^0 - k_{PP} Y_0 Q_3^0 + k_t\left(Y_0^0 Y_2^0 + Y_1^0 Y_1^0\right) \tag{A22}$$

Generation 1

$$Y_0^1 = \frac{k_{IP} R_0\left(Q_1^0 + Q_1^1\right) + k_{PP} Y_0^0\left(Q_1^0 + Q_1^1\right)}{k_{PP} Q_1 - k_{PP} Q_1^0 + k_t Y_0} \tag{A23}$$

$$Y_1^1 = \frac{k_P M Y_0^1 + k_{IP} R_0\left(Q_2^0 + Q_2^1\right) + k_{PP}\left[Y_0^0\left(Q_2^0 + Q_2^1\right) + Y_1^0\left(Q_1^0 + Q_1^1\right) + Y_0^1 Q_2^0\right]}{k_{PP} Q_1 - k_{PP} Q_1^0 + k_t Y_0} \tag{A24}$$

$$Y_2^1 = \frac{\begin{array}{l} k_P M\left(2Y_1^1 + Y_0^1\right) + k_{IP} R_0\left(Q_3^0 + Q_3^1\right) + \\ k_{PP}\left[Y_0^0\left(Q_3^0 + Q_3^1\right) + 2Y_1^0\left(Q_2^0 + Q_2^1\right) + Y_2^0\left(Q_1^0 + Q_1^1\right) + Y_0^1 Q_3^0 + 2Y_1^1 Q_2^0\right] \end{array}}{k_{PP} Q_1 - k_{PP} Q_1^0 + k_t Y_0} \tag{A25}$$

$$\frac{dQ_0^1}{dt} = -k_{IP} R_0 Q_1^1 - k_{PP} Y_0 Q_1^1 + k_t Y_0^0 Y_0^1 \tag{A26}$$

$$\frac{dQ_1^1}{dt} = -k_{IP} R_0 Q_2^1 - k_{PP} Y_0 Q_2^1 + k_t\left(Y_0^0 Y_1^1 + Y_0^1 Y_1^0\right) \tag{A27}$$

$$\frac{dQ_2^1}{dt} = -k_{IP} R_0 Q_3^1 - k_{PP} Y_0 Q_3^1 + k_t\left(Y_2^0 Y_0^1 + 2Y_1^0 Y_1^1 + Y_0^0 Y_2^1\right) \tag{A28}$$

Generation 'j' ($1 < j \leq n$)

$$Y_0^j = \frac{k_{IP} R_0 Q_1^j + k_{PP}\left[Y_0^{j-1} Q_1^{j-1} + Q_1^j \sum_{i=0}^{j-1} Y_0^i\right]}{k_{PP} Q_1 - k_{PP} \sum_{i=0}^{j-1} Q_1^i + k_t Y_0} \tag{A29}$$

$$Y_1^j = \frac{\begin{array}{l} k_P M Y_0^j + k_{IP} R_0 Q_2^j + \\ k_{PP}\left[Y_0^{j-1} Q_2^{j-1} + Y_1^{j-1} Q_1^{j-1} + Y_0^j \sum_{i=0}^{j-1} Q_2^i + Q_2^j \sum_{i=0}^{j-1}\left(Y_0^i\right) + Q_1^j \sum_{i=0}^{j-1}\left(Y_1^i\right)\right] \end{array}}{k_{PP} Q_1 - k_{PP} \sum_{i=0}^{j-1} Q_1^i + k_t Y_0} \tag{A30}$$

$$Y_2^j = \frac{k_{PP}\left[\begin{array}{l} k_P M\left(2Y_1^j + Y_0^j\right) + k_{IP} R_0 Q_3^j + \\ Y_0^{j-1} Q_3^{j-1} + 2Y_1^{j-1} Q_2^{j-1} + Y_2^{j-1} Q_1^{j-1} + \\ Y_0^j \sum_{i=0}^{j-1} Q_3^i + 2Y_1^j \sum_{i=0}^{j-1} Q_2^i + Q_3^j \sum_{i=0}^{j-1}\left(Y_0^i\right) + 2Q_2^j \sum_{i=0}^{j-1}\left(Y_1^i\right) + Q_1^j \sum_{i=0}^{j-1}\left(Y_2^i\right) \end{array}\right]}{k_{PP} Q_1 - k_{PP} \sum_{i=0}^{j-1} Q_1^i + k_t Y_0} \tag{A31}$$

$$\frac{dQ_0^j}{dt} = -k_{IP}R_0Q_1^j - k_{PP}Y_0Q_1^j + k_t\left(\frac{1}{2}Y_0^{j-1}Y_0^{j-1} + Y_0^j\sum_{i=0}^{j-1}Y_0^i\right) \quad \text{(A32)}$$

$$\frac{dQ_1^j}{dt} = -k_{IP}R_0Q_2^j - k_{PP}Y_0Q_2^j + k_t\left(Y_1^{j-1}Y_0^{j-1} + Y_1^j\sum_{i=0}^{j-1}Y_0^i + Y_0^j\sum_{i=0}^{j-1}Y_1^i\right) \quad \text{(A33)}$$

$$\frac{dQ_2^j}{dt} = -k_{IP}R_0Q_3^j - k_{PP}Y_0Q_3^j + k_t\left(\begin{array}{l} Y_2^{j-1}Y_0^{j-1} + Y_1^{j-1}Y_1^{j-1} + Y_0^j\sum_{i=0}^{j-1}Y_2^i + \\ 2Y_1^j\sum_{i=0}^{j-1}Y_1^i + Y_2^j\sum_{i=0}^{j-1}Y_0^i \end{array}\right) \quad \text{(A34)}$$

Closure approximation to the third moment [36]:

$$Q_3^i = 2\frac{Q_2^iQ_2^i}{Q_1^i} + \frac{Q_2^iQ_1^i}{Q_0^i} \quad \text{(A35)}$$

Four generations were used in the simulations (n = 4).

### A4. Balance of sequences

**Table A1**
Reactions in terms of sequences

| Reaction | Chemical equation |
|---|---|
| EGDMA initiation | $R_0 + M_2 \xrightarrow{k_{i2}} L_{1,2}$ |
| $L_1$ generation by EGDMA propagation | $R_{r,i} + M_2 \xrightarrow{k_{pi2}} L_{1,2}$; i = 1-3 |
| Sequence growth | $L_{r,i} + M_j \xrightarrow{k_{pij}} L_{r+1,j}$; i = 1–3; j = 1-2 |
| PDB initiation | $L_{r,i} + R_0 \xrightarrow{k_{i3}} F$; i = 1-3 |
| Cross-linking | $L_{r,j} + R_{r,i} \xrightarrow{k_{pi3}} F$; i = 1–3; j = 1-3 |
| Sequence termination | $R_{s,i} + L_{r,j} \xrightarrow{k_t} F$; i = 1–3; j = 1-3 |
| Cyclization | $L_{r,i} \xrightarrow{k^C_{pi3,r}} Cy_r$; i = 1-3 |

F: Polymer fragment.

$$L_1 = \frac{M_2\left(k_{i2}R_0 + Y_0\sum_{i=1}^3 k_{pi2}f_{Ri}\right)}{M_1\sum_{i=1}^3 k_{pi1}f_{Ri} + M_2\sum_{i=1}^3 k_{pi2}f_{Ri} + PDB\sum_{i=1}^3 k_{pi3}f_{Ri} + k_{i3}R_0 + Y_0\sum_{i=1}^3 k_{pi3}f_{Ri} + k_tY_0} \quad \text{(A36)}$$

$$L_r = \frac{L_{r-1}\left[M_1\sum_{i=1}^3 k_{pi1}f_{Ri} + M_2\sum_{i=1}^3 k_{pi2}f_{Ri} + PDB\sum_{i=1}^3 k_{pi3}f_{Ri}\right]}{M_1\sum_{i=1}^3 k_{pi1}f_{Ri} + M_2\sum_{i=1}^3 k_{pi2}f_{Ri} + PDB\sum_{i=1}^3 k_{pi4}f_{Ri} + k_{i3}R_0 + Y_0\sum_{i=1}^3 k_{pi3}f_{Ri} + k_tY_0 + k^C_{p,r}} \quad \text{(A37)}$$

$$k^C_{pi,3} = \frac{k_{pi3}}{k_{p13}}k^C_{p1,3}\ (1 \le i \le 3) \quad \text{(A38)}$$

$$k^C_{p,r} = \sum_{i=1}^3 k^C_{pi,r}f_{Ri} \quad \text{(A39)}$$

$$RC = \sum_{r=1}^m k^C_{p,r}L_r \quad \text{(A40)}$$

A correlation between cyclization rate coefficients was considered by using Rolfes and Stepto equation [37], as follows.

$$k^C_{pi,r} = \left(\frac{2}{r-1}\right)^{1.5}k^C_{pi,3}\ (1 \le i \le 3) \quad \text{(A41)}$$

In this work, it was considered that cyclizable sequences have a number of monomer units between 3 and m ($3 \le r \le m$). The maximum number of units considered for the sequences (m) was 10. Details about the balance of sequences can be found in Ref. [38].

$$W_g = \frac{Q_1 - \sum_{i=0}^n Q_1^i}{Q_1} \quad \text{(A42)}$$

$$X = \frac{U_1 + U_2}{M_{1,0} + M_{2,0}} \quad \text{(A43)}$$

$$U_1 = M_{1,0} - M_1 \quad \text{(A44)}$$

$$U_2 = M_{2,0} - M_2 \quad \text{(A45)}$$

## Symbology

| | |
|---|---|
| $A_1$ | Coiling parameter for polymer chains in the toluene/heptane solution |
| $A_2$ | Coiling parameter for dry polymer |
| $A_3$ | Coiling parameter for polymer chains in THF |
| $Cy_r$ | Cyclic segment with 'r' monomer units |
| F | Polymer fragment |
| $f_{Mj}$ | Mole fraction of type 'j' monomers related to the total amount of monomers |
| I | Initiator |
| $k^C_{pi,r}$ | Rate constant of cyclization for a sequence containing a type 'i' radical center and 'r' monomeric units ($s^{-1}$) |
| $f_{Ri}$ | Mole fraction of radicals of type 'i' related to the total number of radicals |
| G | Concentration of elementary gel structures (mol $L^{-1}$) |
| $k_{CG}$ | Global rate constant of combination of elementary gel structures (L $mol^{-1}$ $s^{-1}$) |
| $k_{CG0}$ | Intrinsic rate constant of combination of elementary gel structures (L $mol^{-1}$ $s^{-1}$) |
| $k_d$ | Rate constant of initiator decomposition ($s^{-1}$) |
| $k_I$ | Pseudo-kinetic rate constant for monomer initiation (L $mol^{-1}$ $s^{-1}$) |

$k_{Ij}$ Rate constant of initiation for the monomer of type 'j' (L $mol^{-1}$ $s^{-1}$)
$k_{IP}$ Pseudo-kinetic rate constant for PDB initiation (L $mol^{-1}$ $s^{-1}$)
$k_P$ Pseudo-kinetic rate constant of monomer propagation (L $mol^{-1}$ $s^{-1}$)
$k^*_{p13}$ Diffusion-controlled rate constant of cross-linking (L $mol^{-1}$ $s^{-1}$)
$k_{pij}$ Rate constant of intermolecular propagation between a radical of type 'i' and a monomer of type 'j' (L $mol^{-1}$ $s^{-1}$)
$k_{PP}$ Pseudo-kinetic rate constant for PDBs propagation (L $mol^{-1}$ $s^{-1}$)
$k_t$ Rate constant of termination by combination (L $mol^{-1}$ $s^{-1}$)
$k^*_t$ Diffusion-controlled rate constant of termination (L $mol^{-1}$ $s^{-1}$)
$L_r$ Sequence containing 'r' monomer units
$L_{r,i}$ Sequence containing 'r' monomer units and a radical of type 'i'
m Maximum number of monomeric units considered for the sequences
M Total monomer concentration (mol $L^{-1}$)
$M_i$ Monomer of type 'i' (i: 1 = Styrene, 2 = EGDMA)
$M_{i,0}$ Initial concentration of the monomer of type 'i'
$M_G$ Weight-average molecular weight of the elementary gel structures (g $mol^{-1}$)
$\overline{M_M}$ Average molecular weight of monomeric units (g $mol^{-1}$)
n Total number of generations considered in the numerical fractionation method
PDB Total pendant double bonds
$P_r$ Dead polymer molecule containing 'r' monomeric units
$Q_j$ Moment of order 'j' for the overall dead polymer
$Q^i_j$ Moment of order 'j' for dead polymer from generation 'i'
R Universal gas constant, 8.314 J/(mol.K)
$R_0$ Primary radical
RC Rate of cyclization (mol $L^{-1}s^{-1}$)
$R_{g1}$ Radius of gyration for chains in solution (nm)
$R_{g2}$ Radius of gyration for dry polymer (nm)
$R_r$ Polymeric radical containing 'r' monomeric units
$R_{r,i}$ Polymeric radical of type 'i', containing 'r' monomeric units
SA Specific surface area of the polymer particles ($m^2$/g)
Sw Swelling index
T Reaction temperature
$U_i$ Monomeric unit of type 'i'
$V_P$ Fixed pore volume ($cm^3$/g)
$V_{sw}$ Experimental volume of swollen gel ($cm^3$/g)
$V^p_{sw}$ Predicted volume of swollen gel ($cm^3$/g)
$w_d$ Weight of dried sample (g)
$W_g$ Weight fraction of gel (g)
$w_{HQ}$ Weight of hydroquinone added to the sample (g)
$w_s$ Weight of collected sample (g)
$w_{sw}$ Weight of swollen gel (g)
X Monomer conversion
$Y_{EGDMA}$ Molar fraction of EGDMA in the monomer mixture
$Y_M$ Volumetric fraction of monomers in the organic phase
$y_{Mon}$ Weight fraction of monomers in the total content fed to the reactor
$y_{PVA}$ Weight fraction of PVA in the total content fed to the reactor
$Y_{TOL}$ Volumetric fraction of toluene in the toluene/heptane mixture
$\beta_1$ Proportionality coefficient for the radius of gyration of EGS in the toluene/heptane solution
$\beta_2$ Proportionality coefficient for the radius of gyration of EGS in the dry state
$\beta_3$ Proportionality coefficient for the radius of gyration of EGS in THF
$\gamma_1$ Linear coefficient of $\beta_1$ equation
$\gamma_2$ Exponent of $\beta_1$ equation
$\rho_{CL}$ Cross-linking density (g/$cm^3$)
$\rho_P$ Copolymer density (g/$cm^3$)
$\varphi$ Conversion factor

## References


[1] I.M. Abrams, J.R. Millar, A history of the origin and development of macroporous ion-exchange resins, React. Funct. Polym. 35 (1997) 7–22.
[2] R.A. Beauvais, S.D. Alexandratos, Polymer-supported reagents for the selective complexation of metal ions: an overview, React. Funct. Polym. 36 (1998) 113–123.
[3] G.B. Fahs, S.D. Benson, R.B. Moore, Blocky sulfonation of syndiotactic polystyrene: a facile route toward tailored ionomer architecture via post-polymerization functionalization in the gel state, Macromolecules 50 (2017) 2387–2396.
[4] S. Lux, T. Winkler, G. Berger, M. Siebenhofer, Kinetic study of the heterogeneous catalytic esterification of acetic acid with methanol using Amberlyst®15, Chem. Biochem. Eng. Q. 29 (2015) 549–557.
[5] R. Soto, C. Fité, E. Ramírez, R. Bringué, F. Cunill, Equilibrium conversion, selectivity and yield optimization of the simultaneous liquid-phase etherification of isobutene and isoamylenes with ethanol over Amberlyst™ 35, Fuel Process. Technol. 142 (2016) 201–211.
[6] R. Suresh, J.V. Antony, R. Vengalil, G.E. Kochimoolayil, R. Joseph, Esterification of free fatty acids in non- edible oils using partially sulfonated polystyrene for biodiesel feedstock, Industrial Crops Prod. 95 (2017) 66–74.
[7] L.G. Aguiar, E.F. Souza, R. Giudici, Kinetic modeling of the copolymerization of acrylic acid and trimethylolpropane triacrylate over pre and post-gelation periods, Eur. Polym. J. 74 (2016) 264–278.
[8] S. Hamzehlou, Y. Reyes, J.R. Leiza, Quantitative study on the homogeneity of networks synthesized by nitroxide-mediated radical copolymerization of styrene and divinylbenzene, Eur. Polym. J. 85 (2016) 244–255.
[9] V.N. Santos, L.G. Aguiar, R. Giudici, Autoacceleration and cyclization effects on styrene/divinylbenzene copolymerization, Macromol. React. Eng. (2016) 11, http://dx.doi.org/10.1002/mren.201600021.
[10] L.G. Aguiar, Styrene–dimethacrylate copolymerization kinetic modeling, Polym. Int. 65 (2016) 142–151.
[11] D.S.A. Achilias, Review of modeling of diffusion controlled polymerization reactions, Macromol. Theory Simul. 16 (2007) 319–347.
[12] J.C. Hernández-Ortíz, E. Vivaldo-Lima, L.M.F. Lona, N.T. McManus, A. Penlidis, Modeling of the nitroxide-mediated radical copolymerization of styrene and divinylbenzene, Macromol. React. Eng. 3 (2009) 288–311.
[13] J.X. Jiang, F. Su, A. Trewin, C.D. Wood, H. Niu, J.T.A. Jones, Y.Z. Khimyak, A.I. Cooper, Synthetic control of pore dimension and surface area in conjugated microporous polymer and copolymer networks, J. Am. Chem. Soc. 130 (2008) 7710–7720.
[14] S. Xu, K. Song, T. Li, B. Tan, Palladium catalyst coordinated in knitting N-heterocyclic carbene porous polymers for efficient Suzuki–Miyaura coupling reactions, J. Mat. Chem. A 3 (2015) 1272–1278.
[15] H. Li, Z. Fu, C. Yan, J. Huang, Y.N. Liu, S.I. Kirin, Hydrophobic-hydrophilic post-cross-linked polystyrene/poly(methyl acryloyl diethyleneriamine) interpenetrating polymer networks and its adsorption properties, J. Coll. Interf. Sci. 463 (2016) 61–68.
[16] K. Golker, I.A. Nicholls, The effect of crosslinking density on molecularly imprinted polymer morphology and recognition, Eur. Polym. J. 75 (2016) 423–430.
[17] L.G. Aguiar, Mathematical modeling of the internal surface area of copolymer particles based on elementary gel structures, Macromol. React. Eng. 10 (2016) 588–599.
[18] O. Okay, Macroporous copolymer networks, Polym. Prog. Sci. 25 (2000) 711–779.
[19] L.G.A. Aguiar, Cross-linking copolymerization mathematical model including phase separation and cyclization kinetics, Macromol. Theory Simul. 24 (2015) 176–180.
[20] F.M.B. Coutinho, M.A. Neves, M.L. Dias, Porous structure and swelling properties of styrene-divinylbenzene copolymers for size-exclusion chromatography, J. Appl. Polym. Sci. 65 (1997) 1257–1262.
[21] O.E. Akbay, M.R. Altıokka, Kinetics of esterification of acetic acid with n-amyl alcohol in the presence of Amberlyst-36, Appl. Cat. A 396 (2011) 14–19.
[22] S. Brunauer, P.H. Emmett, E.J. Teller, Am. Chem. Soc. 60 (1938) 309–319.
[23] D. Rabelo, F.M.B. Coutinho, Porous structure formation and swelling properties of styrene–divinylbenzene copolymers–effect of diluent nature, Macromol. Symp. 84 (1994) 341.
[24] D. Rabelo, F.M.B. Coutinho, Structure and properties of styrene-

divinylbenzene copolymers, Polym. Bull. 30 (1993) 725.
[25] Y. Saka, P.B. Zetterlund, M. Okubo, Gel formation and primary chain lengths in nitroxide-mediated radical copolymerization of styrene and divinilbenzene in miniemulsion, Polymer 48 (2007) 1229–1236.
[26] A.J. Scott, A. Nabifar, J.C. Hernández-Ortíz, N.T. McManus, E. Vivaldo-Lima, A. Penlidis, Crosslinking nitroxide-mediated radical copolymerization of styrene with divinilbenzene, Eur. Polym. J. 51 (2014) 87–111.
[27] J. Rigolini, D. Brassl, S. Reynaud, L. Billon, Microwave assisted nitroxide-mediated polymerization for water-soluble homopolymers and block copolymers synthesis in homogeneous aqueous solution, J. Polym. Sci. A 48 (2010) 5775–5782.
[28] L.G. Aguiar, M.A.D. Gonçalves, V.D. Pinto, R.C.S. Dias, M.R.P.F.N. Costa, R. Giudici, Mathematical modeling of NMRP of styrene–divinylbenzene over the pre-and post-gelation periods including cyclization, Macromol. React. Eng. 8 (2014) 295–313.
[29] M.A.D. Gonçalves, V.D. Pinto, R.C.S. Dias, M.R.P.F.N. Costa, L.G. Aguiar, R. Giudici, Gel Formation in aqueous suspension nitroxide-mediated radical Co-Polymerization of styrene/divinylbenzene, Macromol. React. Eng. 7 (2013) 155–175.
[30] M.A.D. Gonçalves, I.M.R. Trigo, R.C.S. Dias, M.R.P.F.N. Costa, FTIR-ATR monitoring and SEC/RI/MALLS characterization of ATRP synthesized hyperbranched polyacrylates, Macromol. Symp. 291 (2010) 239–250.
[31] J. Brandrup, E.H. Immergut, E.A. Grulke, Polymer Handbook, Wiley, New York, 2003.
[32] A.C. Shah, I.W. Parsons, R.N. Haward, Study of dimethacrylates as crosslinkers for Styerene, Polymer 19 (1978) 1067–1074.
[33] A.C. Shah, I.W. Parsons, R.N. Haward, Dillute gelling systems: copolymers of styrene and glycol dimethacrylates, Polymer 21 (1980) 825–828.
[34] M. Imoto, T. Otsu, T. Ota, Kinetics of the polymerization of styrene catalyzed by benzoyl peroxide and dimethylaniline. VIII. On vinyl polymerization, Macromol. Chem. Phys. 16 (1954) 10–20.
[35] L.J. Fetters, N. Hadjichristidis, J.S. Lindner, J.W. Mays, Molecular weight dependence of hydrodynamic and thermodynamic properties for well-defined linear polymers in solution, J. Phys. Chem. Ref. Data 23 (1994) 619–640.
[36] G.M. Saidel, S. Katz, Emulsion polymerization: a stochastic approach to the polymer size distribution, J. Polym. Sci. Ps. 27 (1969) 149–169.
[37] H. Rolfes, R.F.T. Stepto, Network formation and properties: rate theory description of effects of ring formation on elastic shear modulus of RA2 + RB3 networks, Makromol. Chem. Macromol. Symp. 40 (1990) 61–79.
[38] L.G. Aguiar, M.A.D. Gonçalves, V.D. Pinto, R.C.S. Dias, M.R.P.F.N. Costa, R. Giudici, Development of cyclic propagation kinetics for modeling the nitroxide-mediated radical copolymerization of styrene-divinylbenzene, Macromol. React. Eng. 8 (2014) 282–294.